The Journal of Engine Research

Journal Homepage: www.engineresearch.ir
DOI:10.22034/ER.2022.697928

Study of GDI injector in constant volume chamber by optical measurements and CFD-Simulation

A. Asef[1], A. Mohammadi[2*], V. Khorramirad[3], N. Ajami[4], A. H. Parivar[5], K. Maghsoudi Mehraban[6]

[1] *Irankhodro Powertrain Company (IPCO), Tehran, Iran, a_asef@ip-co.com*
[2] *Faculty of Mechanical Engineering Department, Shahid Rajaee Teacher Training University, amohammadi@sru.ac.ir*
[3] *Irankhodro Powertrain Company (IPCO), Tehran, Iran, v_khorami@ip-co.com*
[4] *Irankhodro Powertrain Company (IPCO), Tehran, Iran, n_ajami@ip-co.com*
[5] *Irankhodro Powertrain Company (IPCO), Tehran, Iran, a_parivar@ip-co.com*
[6] *Faculty of Mechanical Engineering Department, Shahid Rajaee Teacher Training University, maghsoudi@sru.ac.ir*

[*] *Corresponding Author*

ARTICLE INFO

Article history:
Received: 04 February 2022
Accepted: 19 May 2022

Keywords:
GDI
Injector
Optical
CFD

ABSTRACT

Better performance and the regulatory requirements concerning combustion emissions have caused downsized GDI engines and consideration of strategies for improving in-cylinder mixture preparation. The sprays characteristics of the fuel injectors of GDI engines have been widely investigated by researchers. The interest in studying the characteristics of the spray is due to a strong relationship with the subsequent combustion reaction and thus with the engine's thermal efficiency. This paper analyzes the mixture formation of the spray employing an experimental laser apparatus that was used to measure the spray penetration in a constant volume chamber (CVC) and simulations performed by the fast response CFD CONVERGE software. The fuel injector used in the tests was a six-hole direct injection injector with iso-octane fuel. The measurements were taken 100 mm downstream from the injector tip along the axis with 20 MPa injection pressure. During experiments, it was observed that spray development is not symmetrical with the vertical axis, and with decreasing chamber pressure, it develops faster. Moreover, the average spray development velocities in simulations are in good agreement with experimental results.

1) Introduction

The GDI engines have been produced since 1990 [1]. Currently, GDI development focuses on further improvement of combustion processes and engine downsizing [2]. The benefits of GDI include more precise fuel mixture control and improved transient response [3]. Recently, several injector manufacturers have designed second-generation systems which produce stable fuel sprays with fine fuel droplets [4]. Multi-hole injectors have been investigated due to their potential for good fuel stratification, thus being able to extend the lean limit further [5,6]. The challenge in GDI engines is to prepare fuel-air mixture towards the spark plug over the full range of engine operating [7,8].

Figure 1 displays the progression of the GDI high-pressure fuel system, since its market introduction in the mid-Nineties. These systems supported stratified combustion and operated in the range of 10 MPa fuel system pressure.

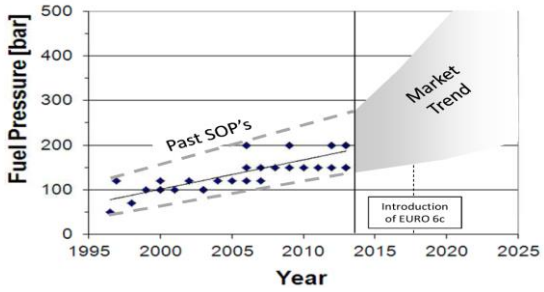

Figure 1: Pressure Evolution for GDI Systems and Future Trend [3]

Macroscopic spray properties and droplet size distribution for spray coming from a six-hole solenoid GDI fuel injector were studied by R. Kale, et al [9].

In this investigation, three fuels were used: isooctane, ethanol, and n-butanol. The results revealed that a fuel's thermo-physical characteristics, such as saturation temperature, surface tension, density, and viscosity, have a critical influence on spray plume penetration.

R. Kale, et al [10] established an Engine-like hot injector body condition in a constant volume spray chamber. They found that with an increase in injector body temperature, the spray cone angle reduces dramatically. Furthermore, despite dropping the fuel injection pressure from 100 to 40 bar, the droplet size demonstrated a significant reduction in SMD and AMD. Under hot injector body situations, liquid and vapor penetration lengths were found to be increased. Particle image analysis was used to determine the droplet size in this investigation (PIA) by H. Luo [11].

The effects of breakup and coalescence on droplet behavior were examined by varying the injection and ambient pressures. Before impingement, the region towards the center of the spray has larger droplets and a lower droplet number density than the edge, implying that spray breakup and atomization are poor in this area. Under low ambient pressure, the droplet size decreases along with the distance from the wall after impingement. Using a high-pressure gasoline direct injection system, the spray behavior of ethanol fuel was examined by S. S. Patil, et al [12].

The study was conducted with a 3–11 MPa injection pressure and a 1–5 ms injection duration. At 11 MPa injection pressure, the spray penetration length was measured to be 141 mm.

J. Zhou [13] analyzed a fouled (GDI) injector's near-nozzle spray development The study revealed that the interaction between deposits and spray caused multiple undesirable spray behaviors throughout the injection development at all injection pressures studied. Different closely spaced split-injection techniques were used by S. Wu, et al [14] to explore multi-hole and slot gasoline direct-injection (GDI) injectors at various fuel temperatures.

The study showed that the over-penetration issue produced by strong spray collapse at high fuel temperatures of multi-hole GDI injectors can be controlled or avoided by adopting particular injector configurations or split-injection strategies.

B. Lehnert, et al. [15] investigated the characteristics of a high-pressure injector, a GDI injector (maximum fuel pressure of 100 MPa), and an injector of a similar design to a diesel engine. The results showed that the increased fuel pressure reduced the mean and maximum droplet diameters.

Also, jet penetration is not always higher at higher pressures, despite higher injection rates.

2) Experimental setup and method

The constant high-pressure chamber was equipped with a high-pressure multi-hole injector at injection pressures up to 20 MPa and chamber pressures up to 10 Mpa. An

experimental setup of CVC is shown in Figure 2. The experimental setup configuration of the fuel injection system is composed of a hydraulic and electronic system.

Figure 2: Constant volume test chamber and apparatus set-up

The hydraulic system includes a fuel tank with a thermocouple embedded into the tank to read the fuel temperature, an electric fuel pump, a fuel filter, a pressure control valve, and a fuel pressure gauge and is intended to drive the fuel from the tank to the injector. The electronic system houses a pilot injector drive where the injector parameters are programmed and transferred to the injector by a trigger.

The 6-hole injector was installed at the top center of the chamber and its injection duration of 1.5 ms is controlled by the electronic control system. The optical system consists of a compact digital camera Motion Blitz with a maximum resolution of 512 x 512 pixels, enabling it to capture 2500-100000 pictures per second depending on the resolution of photography (Figure 3).

Figure 3: Motion Blitz high-speed camera

Optical measurement techniques used are shadow and Schlieren images. The shadow images show only the liquid fuel whereas the Schlieren images show the liquid and gaseous fuel [4]. To determine the axial penetration a line, perpendicular to the spray axis, is placed at 99 % of the detected spray. The axial penetration is the distance between this limitation and the spray hole.

The chamber pressure and temperature are measured by each test condition. Intake air is supplied through pipelines by valves. System pipelines and pressure regulators were shown in Figure 4.

Figure 4: System pipelines

The iso-octane was used as the test fluid with a working temperature of 25ºC and possible pressures ranging from 1 to 200bar. A schematic test configuration of the test bench is shown in Figure 5.

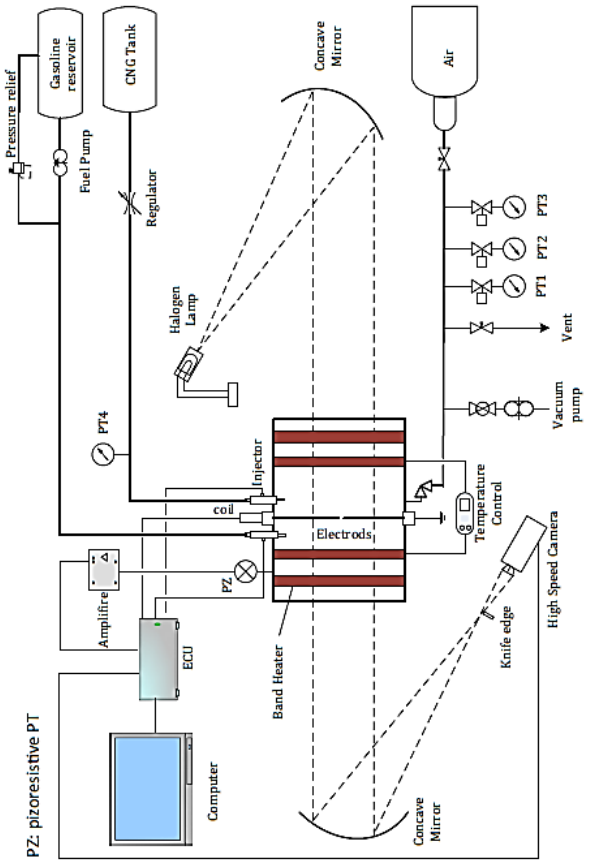

Figure 5: Schematic configuration of test bench [16]

The six-hole GDI injector used in the tests is shown in Figure. 6. The experimental conditions of the test bench are summarized in Table 1.

Figure 6: Six-hole GDI injector

Table 1: Experimental Setup configuration

Injector type	6-hole GDI injector
Chamber dia.×length	135×135 mm
Injection press.	200 bar
Chamber press.	1.5, 4 bar
Chamber temp.	298 K
Fuel	Iso-octane

This study looks into the detailed effect of chamber pressure on the spray characteristics.

3) Spray Structure and Penetration

The spray development of the GDI injector for two-chamber pressure (1.5, 4 bar) is shown in Figures 7 to 12. In Figures 7 to 9 injector socket has a 0-degree angle with CVC horizontal axis, but in figures 10 to 12, it has a 90-degree angle. The Schlieren images show the liquid fuel, and the gaseous fuel is distributed in CVC. The spray develops in the shape of a triangle and the jets linearly develop over time.

At PCVC = 1.5bar, the vaporization phenomena of the outer spray jets appear from 1.3 ms ASOI, and the vaporizing region of outer jets increases inwardly, and primary outward vortices around outer jets are generated, which results from the momentum difference between vaporizing regions of jets. As the CVC decrease

from 4 bar to 1.5 bar, the spray develops more actively due to the bigger momentum of jets with the increasing speed of the spray penetration.

However, on the way of the spray development, from 1.3 ms, the vortices around the end region of the spray are generated earlier than higher chamber pressure due to the larger momentum difference between vaporizing jets. The generation timing of vortices at the end region of the spray is nearly identical and the vaporizing region of jets is much similar with lower chamber pressure conditions. At 2.5 ms, the spray shapes are blunter regardless of fuel injection pressure.

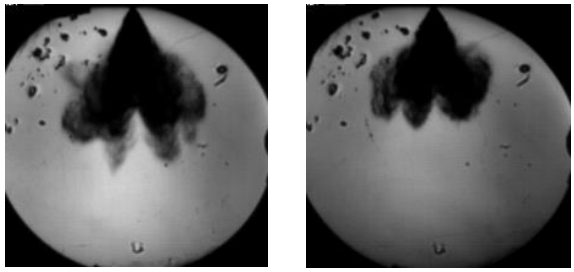

a) b)

Figure 7: spray image 2.2 ms after SOI initial chamber pressure a)1.5 bar and b)4bar

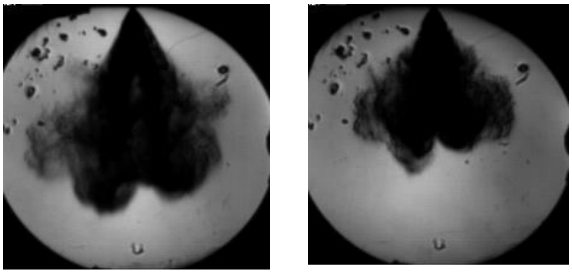

a) b)

Figure 8: Spray image 3.8 ms after SOI initial chamber pressure a)1.5 bar and b)4bar

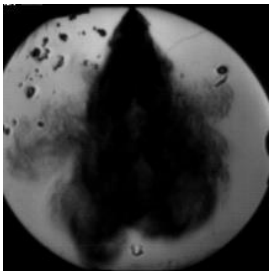

Combustion chamber pressure 1.5 bar
Figure 9a: Spray image 4.9 ms after SOI

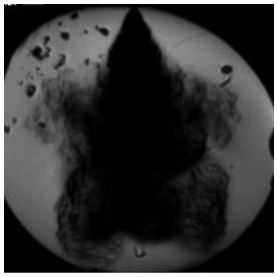

Combustion chamber pressure 4 bar
Figure 9b: Spray image 7.6 ms after SOI

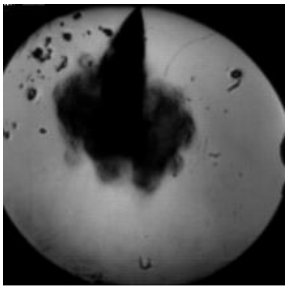

a)

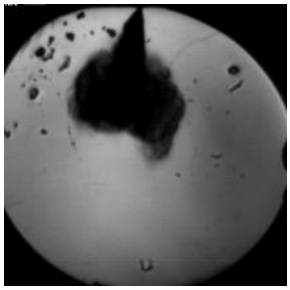

b)

Figure 10: Spray image 2.2 ms after SOI initial chamber pressure a)1.5 bar and b)4bar

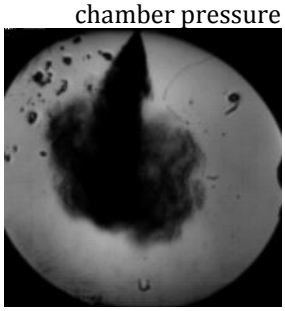

a)

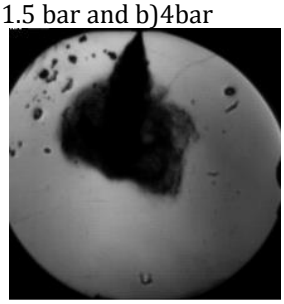

b)

Figure 11: Spray image 3.8 ms after SOI initial chamber pressure a)1.5 bar and b)4bar

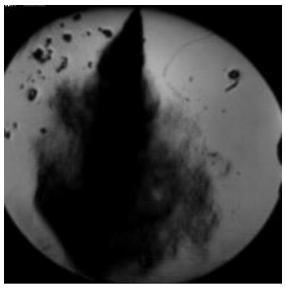

Combustion chamber pressure 1.5 bar
Figure 12a: spray image 5.9 ms after SOI

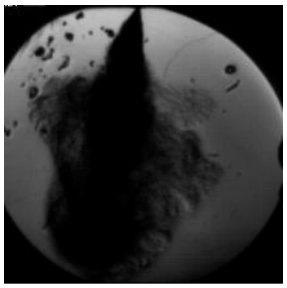

Combustion chamber pressure 4 bar
Figure 12b: spray image 7.6 ms after SOI

4) Governing Equations

In the numerical simulation of spray, it is necessary to simultaneously solve the equations of continuity, species conservation, turbulent fluid flow, energy, fuel injection, and droplets. The Flow continuity equation is written as Equation (1) [17,18]:

$$\frac{\partial \rho}{\partial t} + \nabla.(\rho \vec{v}) = S_{ev} \quad (1)$$

where ρ is the gas's total density, $\vec{v}$is the vector of the gas velocity, $t$is time, and S_{ev} is a source term related to droplet evaporation. Also, the general form of the momentum equation for the flow is expressed as Equation (2) [17,18]:

$$\frac{\partial}{\partial t}(\rho \vec{v}) + \vec{\nabla}.(\rho \vec{v}\vec{v}) = -\nabla p + \nabla.\bar{\tau} + F \quad (2)$$

where p is static pressure and $\bar{\tau}$ is stress tensor and F is an interaction drag force of fuel droplets and the gas phase.

The fluid energy equation is expressed as Equation (3) [17,18].

$$\frac{\partial}{\partial t}(\rho E) + \vec{\nabla}.[\vec{v}(\rho E + p)] = \vec{\nabla}.\left[(k_{eff})\nabla T - \sum_j h_j \vec{J}_j + (\bar{\tau}.\vec{v})\right] + S_e \quad (3)$$

The expression between the brackets on the right side of the Equation includes the heat transfer due to conduction, the enthalpy of the species diffusion, and the dissipation term. Also, $T$is the temperature, $k_{eff}$is the effective thermal conductivity, $E$is the internal energy, $h$is the enthalpy, and $S_e$is the source term related to the heat transfer between the fuel droplets and gas. In particle, energy equations for injection have a phase change term during mixture formation.

Continuity of chemical species of the component i is written as Equation (4) [17,18]:

$$\frac{\partial}{\partial t}(\rho Y_i) + \nabla.(\rho \vec{v} Y_i) = -\nabla.\vec{J}_i + S_i \quad (4)$$

Y_i is the mass fraction, $S_i$is source term and related to fuel evaporation, and $\vec{J}_i$is the diffusion flux. Turbulence is calculated for kinetic energy turbulence (k) and dissipation rate (ε). Here, the standard $k-\varepsilon$ model is used with velocity wall function according to Equations (5) and (6), respectively [17,18].

$$\frac{\partial(\rho k)}{\partial t} + \vec{\nabla}.(\rho \vec{v} k) = -\frac{2}{3}\rho k \vec{\nabla}.\vec{v} + \sigma: \vec{\nabla}\vec{v} + \vec{\nabla}.\left[\left(\frac{\mu}{pr_k}\right)\vec{\nabla}k\right] - \rho\varepsilon + \dot{W}^s \quad (5)$$

$$\frac{\partial(\rho\varepsilon)}{\partial t}+\vec{\nabla}.(\rho\vec{v}\varepsilon) = -\left(\frac{2}{3}C_{\varepsilon 1}-C_{\varepsilon 3}\right)\rho\varepsilon\vec{\nabla}.\vec{v} +\vec{\nabla}.\left[\left(\frac{\mu}{pr_{\varepsilon}}\right)\vec{\nabla}\varepsilon\right]+\frac{\varepsilon}{k}[C_{\varepsilon 1}\sigma:\vec{\nabla}\vec{v}-C_{\varepsilon 2}\rho\varepsilon +C_s\dot{W}^s \quad (6)$$

The effective viscosity value in Equations (5) and (6) is calculated from Equation (7) [17,18].

$$\mu=\mu_m+C_\mu\rho\frac{k^2}{\varepsilon} \quad (7)$$

Where $\sigma:\nabla v=\sigma_{ij}\,{}^{\partial_{vi}}/_{\partial_{xi}}$ is dissipation work and $\dot{W}^s$ is source term due to the droplets injection, pr_k is the turbulent Prandtl number, pr_ε is the Prandtl number of the perturbation kinetic energy dissipation rate, μ_m is the molecular viscosity [17,18].

The dispersion of fuel droplets forms the liquid phase. Therefore, it is possible to apply a random motion perspective in which droplets are considered as a discrete phase. A probability function with eleven variables expresses the droplet distribution. The following function is the probable number of droplets per unit volume at a given location x, time t, at velocities between u and $u+du$, at radius between r and $r+dr$, at temperatures between T and $T+dT$, and droplet distortion parameters between y and $y+dy$ between $\dot{y}$ and expresses $\dot{y}+d\dot{y}$:

$$f(x,u,t,r,T,y,\dot{y})dxdudtdrdTdyd\dot{y}$$

The probability survival equation is expressed by Equation (8) [17,18]. The source terms $\dot{f}_{co}$ and $\dot{f}_{br}$ are related to the collision and breakup of the droplets, respectively. Eulerian phase source terms are determined by summing the changes in mass, momentum, and energy of the droplets at the location x and t of time.

where g is the acceleration of gravity, I_1 is the internal energy, C_1 is the specific heat, and v' is the turbulence oscillation of the gas velocity.

$$\frac{\partial f}{\partial t}+\nabla_x.(fu)+\nabla_u.\left(f\frac{\partial u}{\partial t}\right) +\frac{\partial}{\partial t}\left(f\frac{\partial r}{\partial t}\right)+\frac{\partial}{\partial T}\left(f\frac{\partial T}{\partial t}\right) +\frac{\partial}{\partial y}\left(f\frac{\partial y}{\partial t}\right)+\frac{\partial}{\partial \dot{y}}\left(f\frac{\partial \dot{y}}{\partial t}\right)=\dot{f}_{co}+\dot{f}_{br} \quad (8)$$

$$S_{ev}=-\int f\rho 4\pi r^2\frac{\partial r}{\partial t}dudrdTdyd\dot{y} \quad (9)$$

$$S_{mo}=-\int f\rho\left[\frac{4}{3}\pi r^3\left(\frac{\partial u}{\partial t}-g\right)+4\pi r^2\frac{\partial r}{\partial t}u\right]dudrdTdyd\dot{y} \quad (10)$$

$$S_{he}=-\int f\rho\left\{4\pi r^2\left[I_1+\frac{1}{2}(u-v)^2\right]+ \frac{4}{3}\pi r^3\left[C_1\frac{\partial T}{\partial t}+\left(\frac{\partial v}{\partial t}-g\right).(u-v-v')\right]\right\}dvdrdTdyd\dot{y} \quad (11)$$

Since the magnitude of compressive forces and other forces is negligible compared to drag force, only the drag force on the injected droplets (including pressure and viscosity components) is considered for the primary and the secondary breakup of liquid fuel injection [17,18]. The equation of motion of the droplets is as follows (12):

$$\frac{1}{6}\rho_p\pi d^3\frac{du_p}{dt}=\frac{1}{2}(u_g-u_p)|u_g-u_p|\rho_g C_D\frac{\pi d^2}{4} \quad (12)$$

u_p And u_g represent the velocity of the droplets and the velocity of the gas, respectively. C_D is the drag coefficient of the droplets, which is a function of the Reynolds number of the spray stream and is also related to the cross-section of the droplet and is expressed as Equation (13):

$$C_D=\begin{cases}\frac{24}{\mathrm{Re}_p}\left(1+\frac{1}{6}\mathrm{Re}_p^{\frac{2}{3}}\right), & \mathrm{Re}_p<1000\\ 0.424, & \mathrm{Re}_p\geq 1000\end{cases} \quad (13)$$

5) Computational Procedures

Ansys-Fluent solves transient three-dimensional chemically reactive flows with sprays in-cylinder flow and solid-phase calculations. Species, momentum, energy, and turbulence transports equations are solved by the finite volume method. Solutions are marched in several time steps. Viscous, and pressure gradient terms are solved in a coupled and implicit fashion. The solution procedure is a SIMPLE scheme, and each equation is solved iteratively [17, 18]. the flow field is remapped onto a new computational

mesh, which is essentially calculating the convective transport terms.

6) Mesh Generation

Figure 13 shows constant-volume combustion chamber geometry. Before CFD simulation, the computational mesh is generated. The geometry of a mesh is composed of any arbitrary number of logical blocks that are patched together in a completely seamless fashion.

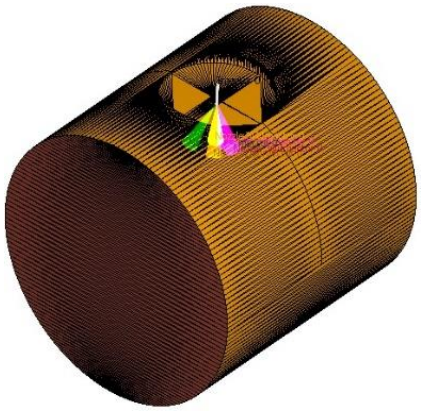

Figure 13: The geometry of constant volume chamber

6) Results and discussion

Figures 14 and 15 present the transient development of the spray front penetration for the various nozzle of the GDI injector and compare it with experimental data extracted from high-speed imaging of the GDI injector. The injection pressure was 20 Mpa and the combustion chamber pressure is 1.5 and 4 bar, respectively. As shown in Figures 14 and 15 the average of spray development velocities in simulations is in good agreement with experimental results. It is notable that, initial deviation of CFD model and experimental results is due to the lack of accurate Injection profile of the Injector in SOI.

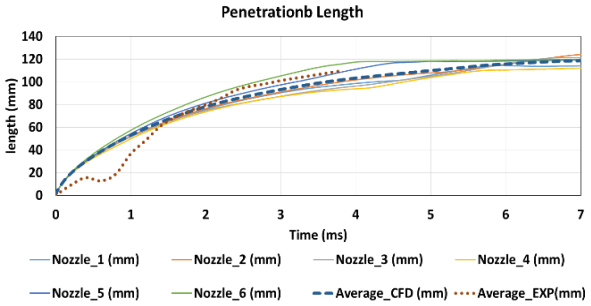

Figure 14: Transient spray penetration for combustion chamber pressure 1.5 bar

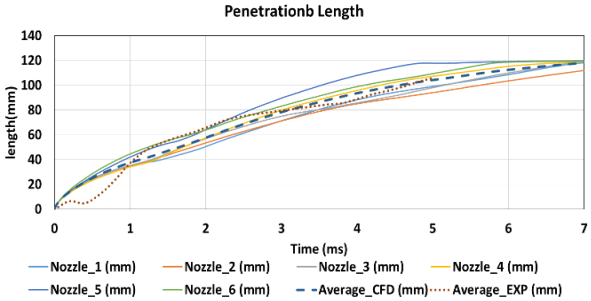

Figure 15: Transient spray penetration for combustion chamber pressure 4 bar

Figure 16 shows a comparison between spray penetration at 2.2, 3.8, and 4.9 ms after the start of injection.

During experiments, it was observed that spray development is not symmetrical with the vertical axis, and with decreasing chamber pressure, it develops faster. Moreover, the average spray development velocities in simulations are in good agreement with experimental results. Notably, deviation of experimental model and simulation, in the beginning, is due to a lack of accurate magnitude of injector needle lift (see Figures 14, 15). For investigation of spray in real injection conditions, temperature and pressure during injection need. Figure. 17 shows in-cylinder pressure and temperature, injection profile versus crank angle. It shows that the average pressure and temperature during injection are 2.9 bar and 650 K respectively.

Figure 18 shows spray penetration with chamber pressure and temperature of 2.9 bar and 650 K, respectively.

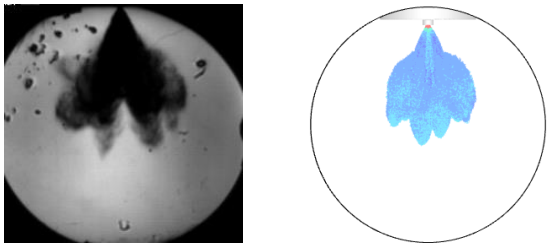

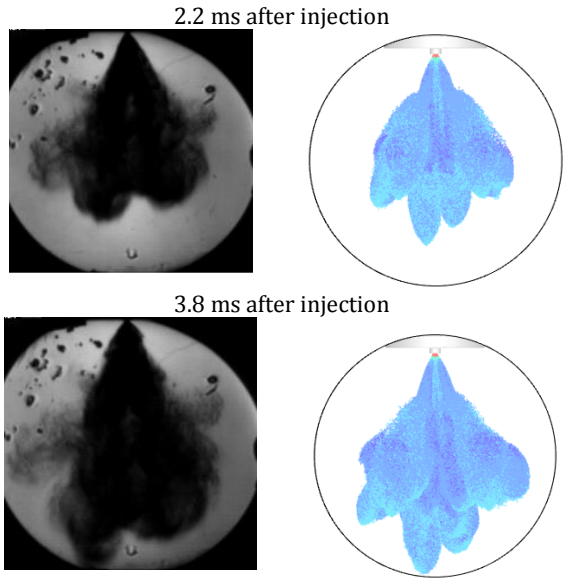

Figure 16: comparison between CFD and test data of spray penetration

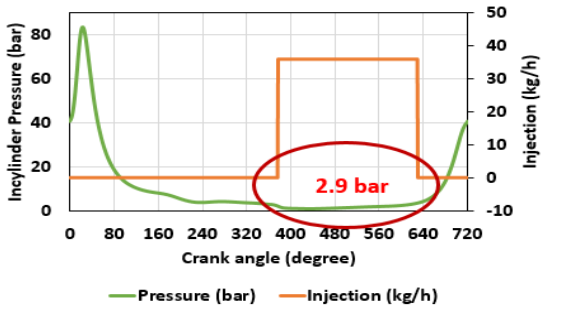

a) in-cylinder pressure and injection profile

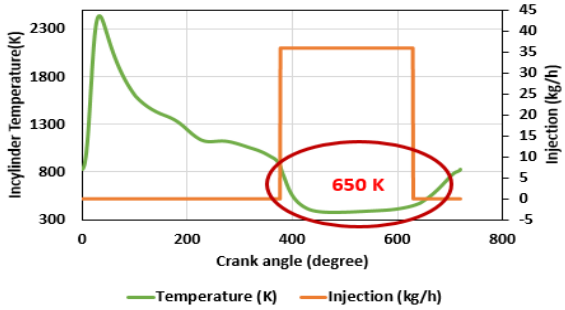

b) in-cylinder temperature and injection profile

Figure 17: In-cylinder and injection profile

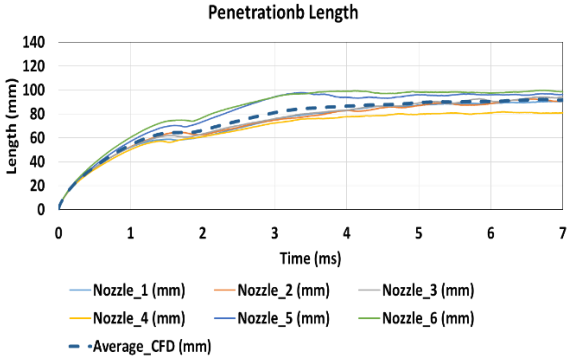

Figure 18: Spray penetration according to real engine conditions

7) Conclusions

The following conclusions are derived from the experimental results and simulation analyses:

- The spray Evolution pattern did not change considerably with increasing chamber pressure.
- Spray penetration of all nozzle is different, so it should be noticed that to avoid spray jet interaction with piston and walls, the nozzle with the highest penetration (nozzle 6 & 5) is critical for this issue.
- The fuel penetration rate was decreased with increasing CVC pressure.
- Fuel penetration has the most evolution in engine condition simulation in the first 1.5 ms compared after that, which means that the evaporation rate is higher after this interval and consequently penetration evolution develops slower.

Acknowledgment

The authors would like to thank IPCO which provides laser experimental apparatus and sponsorship, and the Combustion and Fuel laboratory for their help.

List of Abbreviations

CVC	Constant volume chamber
SOI	Start of Injection
SMD	Sauter mean diameter
AMD	Arithmetic mean diameter

List of Symbols

$C_{\varepsilon_1}, C_{\varepsilon_2}, C_{\varepsilon_3}$	constants
c_p	specific heat at constant pressure
D	Ficks law diffusion coefficient
F^s	rate of momentum gain per unit volume due to spray
g	specific body force (gravity)
h_m	specific enthalpy of species m
I	specific internal energy
J	diffusion flux
k	turbulent kinetic energy
p	fluid pressure
Pr_l	Prandtl number
$\mathrm{Pr}_k, \mathrm{Pr}_\varepsilon, c_\mu$	constant
$\dot{Q}^c$	source term due to chemical heat release
$\dot{Q}^s$	source term due to spray interaction
T	Fluid temperature
u	fluid velocity vector
w	defined velocity in Woschni

	correlation
$\dot{W}^s$	source term due to interaction with spray
y	distance from wall

Greek symbols

δ	Dirac delta function
ε	turbulent dissipation rate
κ	Karmann's constant
λ	thermal conductivity
ν_l	kinematics viscosity of air
ρ_m	mass density of species m
ρ	total mass density
$\dot{\rho}^s$	source term due to spray
σ	viscous stress tensor
Δ	gradient operator

References

[1] J. M. Nouri, and J. H. Whitelaw, Effect of chamber pressure on the spray structure from a swirl pressure atomizer for direct injection gasoline Engines, First International conference on optical diagnostics, London, 16-20 December, 2002

[2] G. K. Fraidl, W. F. Piock and M. Wirth, Gasoline direct injection: actual trends and future strategies for injection and combustion systems, SAE Transactions Journal, vol. 105, pp. 543-559, 1996

[3] N. Mitroglou, J. M. Nouri, M. Gavaises and C. Arcoumanis, Flow and spray characteristics in spray-guided injection engines, Journal Engine Research, vol. 7, no. 3, pp. 255-270, 2006

[4] N. Mitroglou, Multi-hole injectors for direct-injection gasoline engines, PhD Thesis, The City University, pp. 187-248, 2005

[5] N. Mitroglou, J. M. Nouri, Y. Yan, M. Gavaises and C. Arcoumanis, Spray structure generated by multi-hole injectors for gasoline direct injection engines, SAE Technical Paper, pp. 21, 2007

[6] S. Kim, Study on the fuel vapor distribution of the stratified charge in a DISI Engine by PLIF technique, Journal of the Korean Society For Power System Engineering, vol. 12, no. 6, pp. 64-69, 2008

[7] S. Kim, The spray measurements of gasoline, M85, E85, and LPG by a GDI injector in a constant volume chamber, Journal of the Korean Society For Power System Engineering, vol. 16, no. 6, pp. 5-10, 2012

[8] J. M. Nouri, N. Mitroglou, Y. Yan and C. Arcoumanis, Internal flow and cavitation in a multi-Hole injectors for gasoline direct injection engines, SAE Technical Papers 2007

[9] R. Kale, R. Banerjee, Experimental investigation on GDI spray behavior of isooctane and alcohols at elevated pressure and temperature conditions, Journal Fuel, vol. 236, pp. 1-12, 2019

[10] R. Kale, R. Banerjee, Investigation of macroscopic as well as microscopic spray behavior of multi-hole GDI injector under engine like hot injector body conditions, SAE Technical Paper, No. 2018-01-0280, 2018

[11] H. Luo, Microscopic behavior of spray droplets under flat-wall impinging condition, Journal Fuel, vol. 219, pp. 467-476, 2018

[12] S. S. Patil, M. R. Nandgaonkar, Spray behavior analysis of ethanol in Mathematical Modeling, Computational Intelligence Techniques and Renewable Energy: Proceedings of the First International Conference, pp. 207-215, 2020

[13] J. Zhou, Characteristics of near-nozzle spray development from a fouled GDI injector, Journal Fuel, vol. 219, pp. 17-29, 2018

[14] S. Wu, M. Meinhart, J. Yi, Experimental investigation of spray charachteristics of multi-hole and slot GDI injectors at various fuel temperatures using closely spaced split-injectionstragedies, Atomization and Sprays, vol. 29, pp. 522-537, 2019

[15] B. Lehnert, C. Conrad, M. Wensing, GDI sprays with up to 200 MPa Fuel Pressure and Comparison of Diesel-like and Gasoline-Like Injector Designs, SAE Technical Paper, 2020

[16] M. Baloo, B. Mollaei Dariani, Mehdi Akhlaghi, Iman Chitsaz, Effect of iso-octane/methane blend on laminar burning velocity and flame instability, Fuel Journal, Vol. 144, 2015

[17] S. Kazemi, A. Mohammadi, Liquid fuel distribution in the combustion chamber by jet impingement on small cylindrical obstacles, Journal fuel, vol. 134, pp. 3-25, 2021

[18] S. Kazemi, A. mohammdi, liquid fuel distribution in the combustion chamber by jet impingement with small cylindrical obstacles, Journal Fuel combustion, vol. 13, no. 3, pp. 101-119, 2021

فصلنامهٔ علمی تحقیقات موتور

تارنمای فصلنامه: www.engineresearch.ir

DOI:10.22034/ER.2022.697928

مطالعه افشانهٔ موتور تزریق مستقیم در محفظهٔ حجم ثابت با اندازه‌گیری نوری و شبیه‌سازی دینامیک سیالات محاسباتی

علی آصف[۱]، آرش محمدی[۲*]، وحید خرمی راد[۳]، نیما عجمی[۴]، امیر حسین پریور[۵]، کریم مقصودی مهربان[۶]

[۱] شرکت تحقیق، طراحی و تولید موتور ایران خودرو، تهران، ایران، a_asef@ipo-co.com

[۲] عضو هیات علمی دانشکده مهندسی مکانیک دانشگاه تربیت دبیر شهید رجایی، amohammadi@sru.ac.ir

[۳] شرکت تحقیق، طراحی و تولید موتور ایران خودرو، تهران، ایران، v_khorami@ip-co.com

[۴] شرکت تحقیق، طراحی و تولید موتور ایران خودرو، تهران، ایران، n_ajami@ipo-co.com

[۵] شرکت تحقیق، طراحی و تولید موتور ایران خودرو، تهران، ایران، a_parivar@ip-co.com

[۶] عضو هیات علمی دانشکده مهندسی مکانیک دانشگاه تربیت دبیر شهید رجایی، k.maghsoudi@sru.ac.ir

[*] نویسندهٔ مسئول

چکیده

عملکرد بهتر و الزامات نظارتی با توجه به انتشار احتراق باعث کوچک شدن موتور تزریق مستقیم و در نظر گرفتن راهبردهایی برای بهبود آماده‌سازی مخلوط درون استوانه شده است. ویژگی‌های فوارهٔ افشانه‌های سوخت موتورهای تزریق مستقیم به طور گسترده توسط محققان بررسی شده است. علاقه به مطالعه ویژگی‌های فواره‌ها به دلیل رابطه مؤثر با واکنش احتراق و در نتیجه با بازده گرمایی موتور است. این مقاله تشکیل مخلوط فواره را با استفاده از یک دستگاه آزمایشی لیزری مورد استفاده برای اندازه‌گیری نفوذ فواره در محفظهٔ حجم ثابت و شبیه‌سازی‌های انجام شده توسط نرم‌افزار کانورج با پاسخ سریع تحلیل می‌کند. افشانهٔ سوخت مورد استفاده در آزمایش یک افشانهٔ تزریق مستقیم شش سوراخی با سوخت ایزواکتان بود. اندازه‌گیری‌ها در ۱۰۰ میلی‌متر پایین دست از نوک افشانه در امتداد محور با فشار تزریق ۲۰ مگاپاسکال انجام شد. در طول آزمایش‌ها، مشاهده شد که توسعهٔ فواره با محور عمودی قرینه نیست، و با کاهش فشار محفظه، سرعت توسعهٔ آن افزایش می‌یابد. همچنین میانگین سرعت‌های توسعهٔ فواره در شبیه‌سازی‌ها با نتایج تجربی مشابه یکدیگر اند.

اطلاعات مقاله

تاریخچهٔ مقاله:

دریافت: ۱۵ بهمن ۱۴۰۰

پذیرش: ۲۹ اردیبهشت ۱۴۰۱

کلیدواژه‌ها:

تزریق مستقیم بنزین

افشانه

نور

دینامیک سیالات محاسباتی